# Dynamics of a Cubic Nonlinear Vibration Absorber

Shafic S. Oueini, Char-Ming Chin, Ali H. Nayfeh

# Dynamics of a Cubic Nonlinear Vibration Absorber

SHAFIC S. OUEINI, CHAR-MING CHIN, and ALI H. NAYFEH
*Department of Engineering Science and Mechanics (MC 0219), Virginia Polytechnic Institute and State University, Blacksburg, VA 24061, U.S.A.*

**Abstract.** We study the dynamics of a nonlinear active vibration absorber. We consider a plant model possessing curvature and inertia nonlinearities and introduce a second-order absorber that is coupled with the plant through user-defined cubic nonlinearities. When the plant is excited at primary resonance and the absorber frequency is approximately equal to the plant natural frequency, we show the existence of a saturation phenomenon. As the forcing amplitude is increased beyond a certain threshold, the response amplitude of the directly excited mode (plant) remains constant, while the response amplitude of the indirectly excited mode (absorber) increases. We obtain an approximate solution to the governing equations using the method of multiple scales and show that the system possesses two possible saturation values. Using numerical techniques, we perform stability analyses and demonstrate that the system exhibits complicated dynamics, such as Hopf bifurcations, intermittency, and chaotic responses.

**Keywords:** Vibration absorber, saturation, internal resonance, bifurcations.

## 1. Introduction

Nonlinearities are responsible for unusual phenomena in the presence of internal and/or external resonances. Of particular interest are systems coupled with quadratic nonlinearities and possessing a two-to-one internal resonance. Sethna [1] was one of the first researchers to study such systems. He conducted theoretical studies, performed analog simulations, and showed that nonperiodic motions may exist. Theoretical and experimental studies by Nayfeh et al. [2], Haddow et al. [3], and Balachandran and Nayfeh [4] on L-shaped structures have shown that, when two degree-of-freedom systems coupled with quadratic nonlinearities possess a two-to-one internal resonance and the higher mode is subjected to a primary resonance, there exists a saturation phenomenon. When the forcing amplitude exceeds a certain threshold, the amplitude of the directly excited mode remains constant, and the excitation energy is channeled to the unexcited lower mode. As the forcing amplitude increases, the response amplitude of the lower mode increases, while the response amplitude of the higher mode saturates. Bajaj et al. [5] and Banerjee et al. [6] investigated the response of a pendulum mounted on an oscillating mass. They used first- and second-order averaging methods to analyze the dynamics of the system. In addition to reporting the occurrence of periodic and chaotic motions, they found that the saturation phenomenon predicted by the first-order averaging technique is lost when the effect of higher-order nonlinearities is included in the model.

Recently, Oueini et al. [7] and Pratt et al. [8] exploited the saturation phenomenon in devising an active vibration suppression technique. They introduced a second-order absorber and coupled it with the plant through a user-defined quadratic feedback control law. Once the

*Table 1.* Possible feedback signals.

| Sensor | $F_f(t)$ | $F_c(t)$ |
|---|---|---|
| Position | $u_1 u_2^2, \ddot{u}_1 u_2^2$ | $u_2 u_1^2, u_2 \dot{u}_1^2, u_2 \ddot{u}_1^2, u_2 u_1 \ddot{u}_1$ |
| Velocity | $u_1 \dot{u}_2^2, \ddot{u}_1 \dot{u}_2^2$ | $\dot{u}_2 u_1 \dot{u}_1, \dot{u}_2 \dot{u}_1 \ddot{u}_1$ |
| Acceleration | $u_1 \ddot{u}_2^2, \ddot{u}_1 \dot{u}_2^2$ | $\ddot{u}_2 u_1^2, \ddot{u}_2 \dot{u}_1^2, \ddot{u}_2 \ddot{u}_1^2, \ddot{u}_2 u_1 \ddot{u}_1$ |

coupling between the plant and the absorber is established through a sensor and an actuator, effective vibration suppression is achieved by tuning the natural frequency of the absorber to one-half the excitation frequency.

Unlike previous studies that investigated the saturation phenomenon in quadratic systems, we propose to 'reverse-engineer' the saturation phenomenon using cubic terms. We consider a plant modeled by a second-order nonlinear differential equation and introduce an active vibration absorber coupled with the plant via a specific set of cubic nonlinearities. We analyze the resulting equations using the method of multiple scales and show that a saturation phenomenon occurs when a one-to-one internal resonance is imposed between the plant and the absorber. To our knowledge, this is the first instance in which the saturation phenomenon is encountered in cubically coupled systems.

## 2. System Model and Perturbation Solution

The plant is a cantilever beam whose response is governed by a nonlinear partial-differential equation. We consider a mode that is not involved in an internal resonance with any of the other modes. Then, application of a single-mode discretization scheme yields the ordinary-differential equation

$$\ddot{u}_2 + 2\varepsilon^2 \tilde{\mu}_2 \dot{u}_2 + \omega_2^2 u_2 + \tilde{\delta}_1 u_2^3 + \tilde{\delta}_2 \ddot{u}_2 u_2^2 + \tilde{\delta}_3 \dot{u}_2^2 u_2 = \varepsilon^3 F \cos(\Omega t) + \tilde{\alpha}_2 F_c(t), \tag{1}$$

where $u_2$ is the generalized coordinate of the mode under consideration, $\tilde{\mu}_2$ is a damping coefficients, $\omega_2$ is the natural frequency, the $\tilde{\delta}_i$ are constants, $F$ and $\Omega$ are the forcing amplitude and frequency, respectively, $\tilde{\alpha}_2$ is a constant gain, $F_c(t)$ is a control signal, and $\varepsilon$ is a dimensionless bookkeeping parameter. The model includes the curvature nonlinearity $u^3$ and the inertia nonlinearities $\ddot{u}_2 u_2^2$ and $\dot{u}_2^2 u_2$.

We introduce a second-order absorber and couple it with the plant through a user-defined cubic feedback control law. Then, the equation governing the dynamics of the absorber is given by

$$\ddot{u}_1 + 2\varepsilon^2 \tilde{\mu}_1 \dot{u}_1 + \omega_1^2 u_1 = \tilde{\alpha}_1 F_f(t), \tag{2}$$

where $u_1$ is the absorber coordinate and $\tilde{\mu}_1$ and $\omega_1$ are the absorber's damping coefficient and frequency, respectively, $\tilde{\alpha}_1$ is a constant gain, and $F_f(t)$ is a feedback signal. The feedback and control signals may take different forms depending on the available sensor. We list all possible combinations in Table 1. Furthermore, we choose the absorber's frequency such that $\omega_1 \approx \omega_2$ (i.e., one-to-one internal resonance).

We consider the case of primary resonance (i.e., $\Omega \approx \omega_2$) and position feedback and analyze, without loss of generality, the system of equations

$$\ddot{u}_1 + 2\varepsilon^2 \tilde{\mu}_1 \dot{u}_1 + \omega_1^2 u_1 = \alpha_1 \ddot{u}_1 u_2^2, \tag{3}$$

$$\ddot{u}_2 + 2\varepsilon^2 \tilde{\mu}_2 \dot{u}_2 + \omega_2^2 u_2 + \tilde{\delta}_1 u_2^3 + \tilde{\delta}_2 \ddot{u}_2 u_2^2 + \tilde{\delta}_3 \dot{u}_2^2 u_2 = \alpha_2 \dot{u}_1^2 u_2 + \varepsilon^3 F \cos(\Omega t). \tag{4}$$

Using the method of multiple scales [9], we obtain an approximate solution to Equations (3) and (4) in the form

$$u_1 \approx A_1(T_2)\, e^{i\omega_1 T_0} + \overline{A}_1(T_2)\, e^{-i\omega_1 T_0}, \tag{5}$$

$$u_2 \approx A_2(T_2)\, e^{i\omega_2 T_0} + \overline{A}_2(T_2)\, e^{-i\omega_2 T_0}, \tag{6}$$

where $T_0 = t$, $T_2 = \varepsilon^2 t$, and

$$2i\left(\frac{\mathrm{d}A_1}{\mathrm{d}T_2} + \tilde{\mu}_1 A_1\right) + 8\hat{\alpha}_1(2A_2\overline{A}_2 A_1 + \overline{A}_1 A_2^2\, e^{2i\tilde{\sigma}_1 T_2}) = 0, \tag{7}$$

$$2i\left(\frac{\mathrm{d}A_2}{\mathrm{d}T_2} + \tilde{\mu}_2 A_2\right) + 8\delta_e A_2^2\overline{A}_2 + 8\hat{\alpha}_2(-2A_1\overline{A}_1 A_2 + A_1^2\overline{A}_2\, e^{-2i\tilde{\sigma}_1 T_2}) - f\, e^{i\tilde{\sigma}_2 T_2} = 0. \tag{8}$$

Here,

$$\hat{\alpha}_1 = \frac{1}{8}\omega_1\alpha_1, \quad \hat{\alpha}_2 = \frac{1}{8}\omega_1\alpha_2, \quad \tilde{\sigma}_1 T_2 = (\omega_2 - \omega_1)T_0, \quad \tilde{\sigma}_2 T_2 = (\omega_2 - \Omega)T_0,$$

$$\delta_e = \frac{1}{8\omega_2}\left[3\tilde{\delta}_1 - \omega_2^2(3\tilde{\delta}_2 + \tilde{\delta}_3)\right] \quad \text{and} \quad f = \frac{F}{2\omega_2}.$$

To facilitate the analysis, we reduce the number of the parameters in Equations (7) and (8) by introducing the scalings

$$A_1 = c_1 B_1, \quad A_2 = c_2 B_2, \quad \text{and} \quad T_2 = c_3 T, \tag{9}$$

where the $c_i$ are constants. Then, Equations (7) and (8) become

$$2i(B_1' + \mu_1 B_1) + 8\hat{\alpha}_1 c_2^2 c_3(2B_2\overline{B}_2 B_1 + \overline{B}_1 B_2^2\, e^{2i\sigma_1 T}) = 0, \tag{10}$$

$$2i(B_2' + \mu_2 B_2) + 8c_2^2 c_3 \delta_e B_2^2\overline{B}_2$$
$$+ 8\hat{\alpha}_2 c_1^2 c_3(-2B_1\overline{B}_1 B_2 + B_1^2\overline{B}_2\, e^{-2i\sigma_1 T}) - \frac{c_3 f}{c_2}\, e^{i\sigma_2 T} = 0, \tag{11}$$

where

$$\mu_i = c_3\tilde{\mu}_i \quad \text{and} \quad \sigma_i = c_3\tilde{\sigma}_i, \tag{12}$$

and the prime represents differentiation with respect to the time variable $T$. To keep the forcing amplitude $f$ as a bifurcation parameter, we set $c_2 = c_3$. Furthermore, we let

$$\hat{\alpha}_1 c_3^3 = 1 \quad \text{and} \quad \hat{\alpha}_2 c_1^2 c_3 = 1. \tag{13}$$

Solving for the constants, we obtain

$$c_1 = \sqrt{\frac{|\hat{\alpha}_1|^{1/3}}{|\hat{\alpha}_2|}} \quad \text{and} \quad c_2 = c_3 = |\hat{\alpha}_1|^{-1/3}. \tag{14}$$

Moreover, we define

$$\delta = \frac{\delta_e}{\hat{\alpha}_1}. \tag{15}$$

Next, we express $B_1(T)$ and $B_2(T)$ in the polar form

$$B_1 = \frac{1}{2} a_1(T) \, e^{i\beta_1(T)} \quad \text{and} \quad B_2 = \frac{1}{2} a_2(T) \, e^{i\beta_2(T)}. \tag{16}$$

Substituting Equations (14–16) into Equations (10) and (11) and separating real and imaginary parts yields

$$a_1' = -\mu_1 a_1 - a_1 a_2^2 \sin \theta_1, \tag{17}$$

$$a_2' = -\mu_2 a_2 + a_1^2 a_2 \sin \theta_1 + f \sin \theta_2, \tag{18}$$

$$a_1 \beta_1' = a_1 a_2^2 (2 + \cos \theta_1), \tag{19}$$

$$a_2 \beta_2' = \delta a_2^3 + a_1^2 a_2 (\cos \theta_1 - 2) - f \cos \theta_2, \tag{20}$$

where

$$\theta_1 = 2(\beta_2 - \beta_1 + \sigma_1 T) \quad \text{and} \quad \theta_2 = \sigma_2 T - \beta_2. \tag{21}$$

## 3. Equilibrium and Dynamic Solutions

In this section, we study the equilibrium and dynamic solutions of Equations (17–21) and their bifurcations. To determine the equilibrium solutions, we set $a_1' = a_2' = 0$ and $\theta_1' = \theta_2' = 0$ and obtain the algebraic equations

$$\mu_1 a_1 = -a_1 a_2^2 \sin \theta_1, \tag{22}$$

$$\mu_2 a_2 = a_1^2 a_2 \sin \theta_1 + f \sin \theta_2, \tag{23}$$

$$\nu_1 a_1 = a_1 a_2^2 (2 + \cos \theta_1), \tag{24}$$

$$\nu_2 a_2 = \delta a_2^3 + a_1^2 a_2 (\cos \theta_1 - 2) - f \cos \theta_2, \tag{25}$$

where

$$\nu_1 = \sigma_1 + \sigma_2 \quad \text{and} \quad \nu_2 = \sigma_2. \tag{26}$$

There are two possibilities: $a_1 = 0$ and $a_1 \neq 0$. When $a_1 = 0$, it follows from Equations (23) and (25) that

$$[\mu_2^2 + (\nu_2 - \delta a_2^2)^2] a_2^2 - f^2 = 0. \tag{27}$$

This is the single-mode solution. Equation (27) is similar to the frequency-response equation of the forced Duffing oscillator. The unexcited mode does not oscillate while the directly excited mode oscillates with an amplitude that is dependent on the detuning $\nu_2$, the magnitude of the forcing $f$, and the system's initial conditions [10]. When $a_1 \neq 0$, it follows from Equations (22–25) that

$$\mu_1^2 + (\nu_1 - 2a_2^2)^2 - a_2^4 = 0, \tag{28}$$

$$(\mu_1 a_1^2 + \mu_2 a_2^2)^2 + [\nu_2 a_2^2 - a_1^2(\nu_1 - 4a_2^2) - \delta a_2^4]^2 - a_2^2 f^2 = 0, \tag{29}$$

which is a two-mode solution. The solutions of Equation (28) are

$$a_2^{(1)} = \sqrt{\frac{2\nu_1 - \sqrt{\nu_1^2 - 3\mu_1^2}}{3}} \quad \text{and} \quad a_2^{(2)} = \sqrt{\frac{2\nu_1 + \sqrt{\nu_1^2 - 3\mu_1^2}}{3}}. \tag{30}$$

Thus, the directly excited mode may oscillate at two distinct amplitudes that are functions of the detuning parameter $\nu_1$ and the damping coefficient $\mu_1$, but independent of the excitation amplitude $f$. In contrast, the amplitude of the indirectly excited mode is dependent on the excitation amplitude.

To study the stability of the equilibrium solutions, we express $B_1$ and $B_2$ in the form

$$B_1 = \frac{1}{2}(p_1 - iq_1)\,e^{i\nu_1 T} \quad \text{and} \quad B_2 = \frac{1}{2}(p_2 - iq_2)\,e^{i\nu_2 T},\, , \tag{31}$$

where the $p_n$ and $q_n$ are real and write the modulation equations in Cartesian form as

$$p_1' = -\mu_1 p_1 - \nu_1 q_1 + q_1(p_2^2 + 3q_2^2) + 2p_1 p_2 q_2, \tag{32}$$

$$q_1' = -\mu_1 q_1 + \nu_1 p_1 - p_1(q_2^2 + 3p_2^2) - 2q_1 q_2 p_2, \tag{33}$$

$$p_2' = -\mu_2 p_2 - \nu_2 q_2 - q_2(q_1^2 + 3p_1^2) + 2p_1 p_2 q_1 + \delta q_2(p_2^2 + q_2^2), \tag{34}$$

$$q_2' = -\mu_2 q_2 + \nu_2 p_2 + p_2(p_1^2 + 3q_1^2) - 2p_1 q_1 q_2 - \delta p_2(p_2^2 + q_2^2) + f. \tag{35}$$

The stability of a particular equilibrium solution is ascertained by investigating the eigenvalues of the Jacobian matrix of the right-hand sides of Equations (32–35). Then, a pseudo-arclength scheme is used to trace branches of the equilibrium solutions [10, 11].

The purpose of this study is to investigate active implementation of the vibration absorber. In this case, the frequency at which the plant oscillates can be measured, and, accordingly, the frequency of the absorber can be adjusted. Guided by the fact that the amplitudes $a_2^{(1)}$ and $a_2^{(2)}$ in Equation (30) are only functions of $\mu_1$ and $\nu_1$, we choose $\nu_1$ to be a small non-zero number. Consequently, the magnitude of $a_2$ will be constant in both the frequency- and force-response curves. Furthermore, we set the absorber damping coefficient equal to a small but non-zero value.

In Figure 1, we show the frequency-response curves when $\mu_1 = 0.0005$, $\mu_2 = 0.001$, $\nu_1 = 0.01$, $\delta = -1$, and $f = 0.0001$. The plant exhibits a softening-type behavior. In Figure 1b, we illustrate an enlargement of the boxed area labeled 'I' in Figure 1a. Initially, the response consists of the single-mode solution. As $\sigma_2$ is increased beyond the value at point $F$, shown in Figure 1b, and in the presence of large disturbances, a jump to a high-amplitude
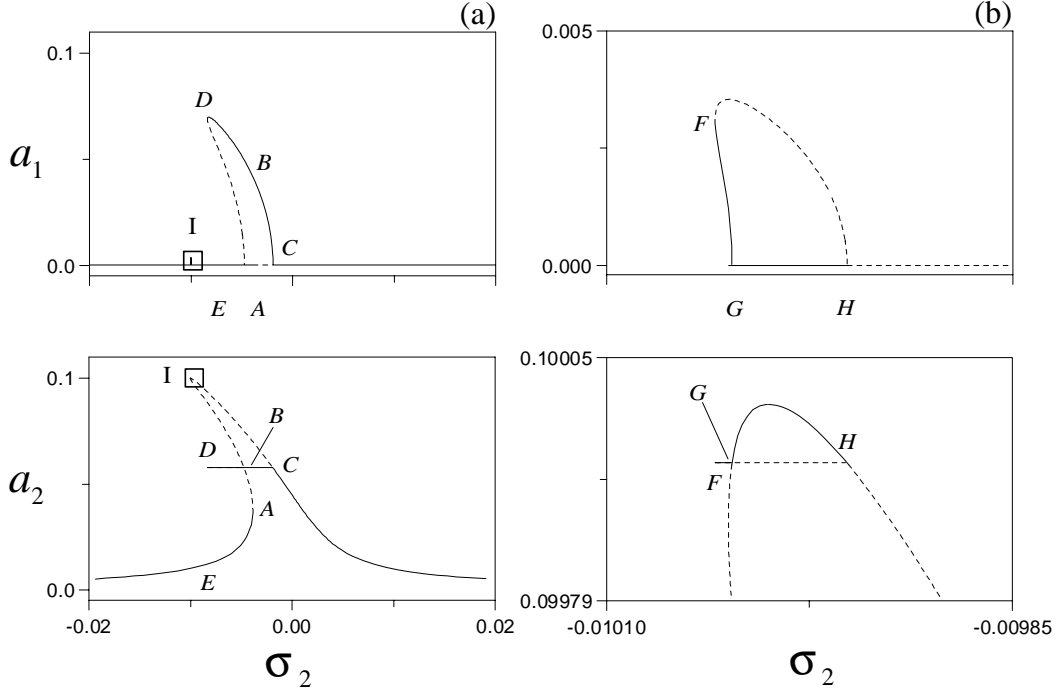
*Figure 1.* Frequency-response curves when $\mu_1 = 0.0005$, $\mu_2 = 0.001$, $\nu_1 = 0.01$, $\delta = -1$, and $f = 0.0001$. (a) Overall frequency-response curves and (b) an enlargement of area 'I'. Solid (dotted) lines denote stable nodes (saddles).

plant response is possible. In this case, the response consists of the two-mode solution along the branch $FG$, and the amplitude of the plant is $a_2^{(2)}$. The two-mode solution experiences a supercritical pitchfork bifurcation at $G$, where the single-mode solution is reached. It is maintained until point $H$, where it undergoes a subcritical pitchfork bifurcation, leading to a jump to the single-mode solution along the branch $EA$. In the absence of large disturbances, the response consists of the single-mode solution, which is stable. At $A$, the single-mode solution undergoes a saddle-node bifurcation, and the response jumps to $B$ where the two-mode solution is sustained. As $\sigma_2$ is increased, the response traces the curve $BC$. Here, the amplitude of the plant is equal to $a_2^{(1)}$. At $C$, the response undergoes a supercritical pitchfork bifurcation after which only the single-mode solution exists. When $\sigma_2$ is decreased from a high value, the single-mode response experiences a supercritical pitchfork bifurcation at $C$, and the resulting two-mode solution traces the curve $CBD$. At $D$, the solution undergoes a saddle-node bifurcation, leading to a jump to point $E$ where the response consists of the single-mode solution thereafter. If $\sigma_2$ is set at a value between the points $H$ and $F$ and a large disturbance is imparted to the system, single- or two-mode solutions may be possible, as discussed previously.

In Figure 2, we show the frequency-response curves when $\mu_1 = 0.0005$, $\mu_2 = 0.001$, $\nu_1 = 0.01$, $\delta = 1$, and $f = 0.0001$. The plant exhibits a hardening-type behavior. In Figure 2b, we illustrate an enlargement of the boxed area labeled 'II' in Figure 2a. As $\sigma_2$ is increased, the response consists of the single-mode solution, which is stable. At point $A$ ($\sigma_2 = 0.001935458$), the response undergoes a subcritical pitchfork bifurcation, which leads to a jump to a two-mode dynamic solution. The dynamic solution is maintained until
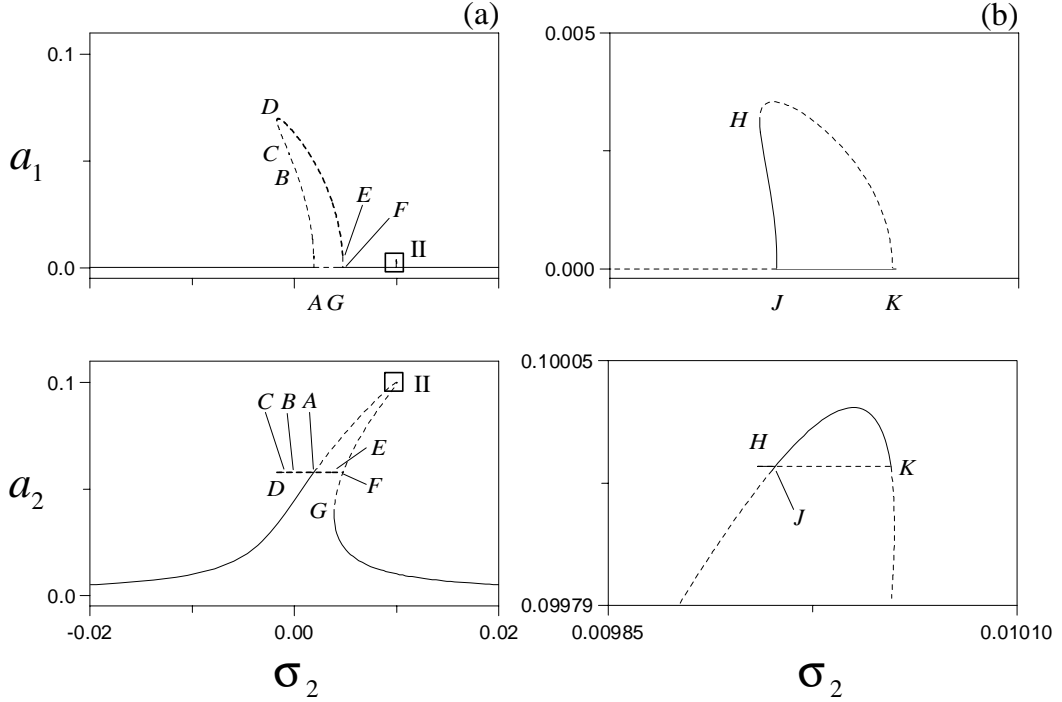
*Figure 2.* Frequency-response curves when $\mu_1 = 0.0005$, $\mu_2 = 0.001$, $\nu_1 = 0.01$, $\delta = 1$, and $f = 0.0001$. (a) Overall frequency-response curves and (b) an enlargement of area 'II'. Solid (dotted) lines denote stable nodes (saddles) and bold-dashed lines denote unstable foci.

$E$ is reached, after which the response jumps to the single-mode solution. The branch $EF$ is unstable (saddle) and, therefore, cannot be attained. Similarly to the case when $\delta = -1$, there exists a region between points $H$ and $K$ where high-amplitude single- or two-mode solutions may be reached in the presence of large disturbances. In the case of reverse sweep and in the absence of large disturbances, the single-mode solution is initially stable. It experiences a saddle-node bifurcation at $G$ ($\sigma_2 = 0.003878544$), leading to a jump to a two-mode dynamic solution. When $\sigma_2$ is in the region $AD$, the dynamic solution coexists with the single-mode solution. When $\sigma_2$ is less than the value at $D$, only the single-mode solution exists.

In Figure 3, we illustrate the loci of the unstable eigenvalues of the two-mode solution shown in Figure 2a as $\sigma_2$ is varied. In Figure 3a, we show the locus of the eigenvalues along the branch $ABCD$. At point $A$, a single eigenvalue goes through zero, indicating a subcritical pitchfork bifurcation. It remains real and positive as $\sigma_2$ is decreased. As point $B$ is approached, two complex conjugate eigenvalues move to the right-hand side of the complex plane. As $\sigma_2$ is decreased further, the real eigenvalue moves to the right until point $C$ is reached, where it reverses direction. At point $D$, it crosses to the left-hand plane through zero, indicating a turning point. Two complex eigenvalues remain in the right-hand side, and the equilibrium solution becomes an unstable focus. In Figure 3b, we illustrate the locus of the unstable eigenvalues for branch $DEF$. As $\sigma_2$ is increased, the imaginary parts of the eigenvalues decrease until they become zero beyond point $E$, where the fixed point becomes a saddle. Then, the remaining two positive real eigenvalues split and move in opposite directions. At point $F$, one eigenvalue is equal to zero, and a non-classical pitchfork bifurcation occurs where the branches of the unstable single and two-mode solutions meet.
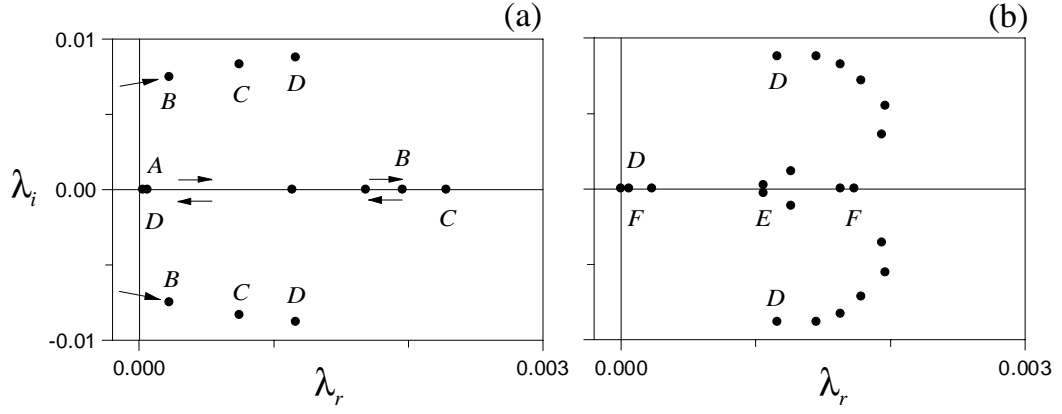
7

*Figure 3.* Loci of the unstable eigenvalues of the two-mode solution when $\mu_1 = 0.0005$, $\mu_2 = 0.001$, $\nu_1 = 0.01$, $f = 0.0001$, and $\delta = 1$. (a) Locus along branch $ABCD$ and (b) locus along branch $DEF$.
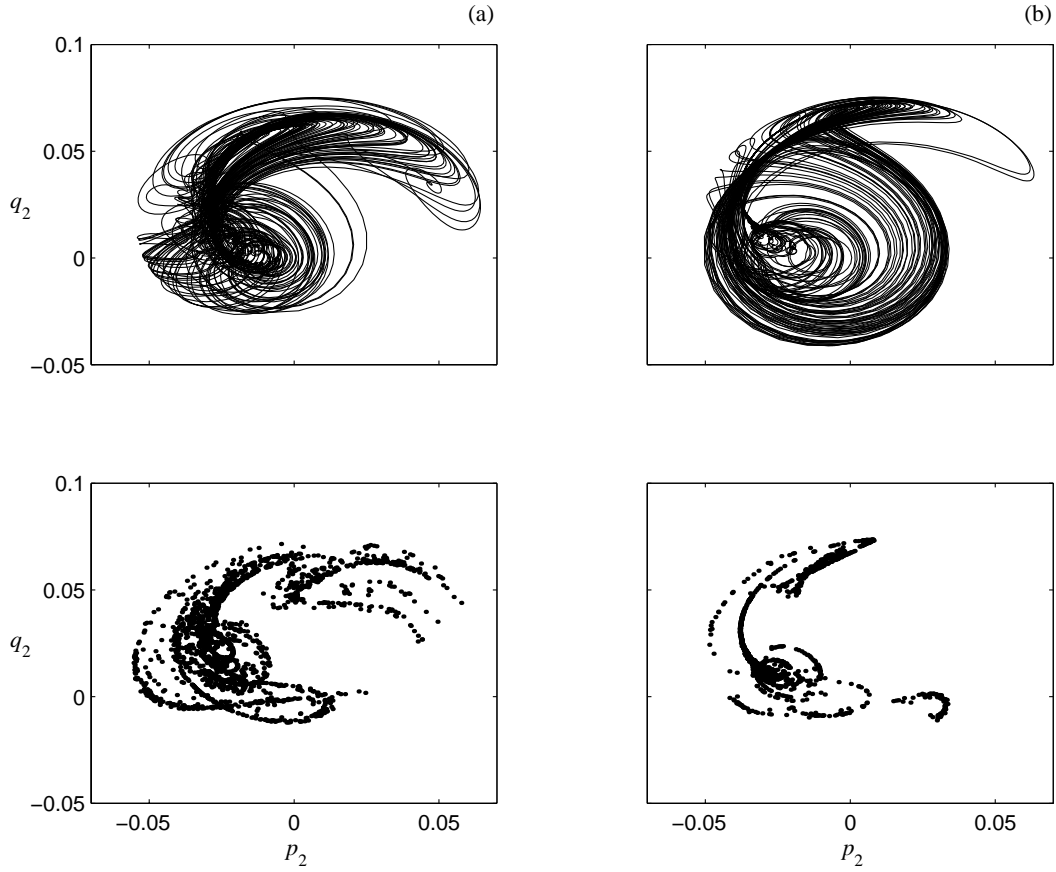


*Figure 4.* Two-dimensional projections of the phase portraits and Poincaré sections of the response when $\delta = 1$, $\mu_1 = 0.0005$, $\mu_2 = 0.001$, $\nu_1 = 0.01$, and $f = 0.0001$. (a) $\sigma_2 = 0.002$ and (b) $\sigma_2 = 0.0036$.
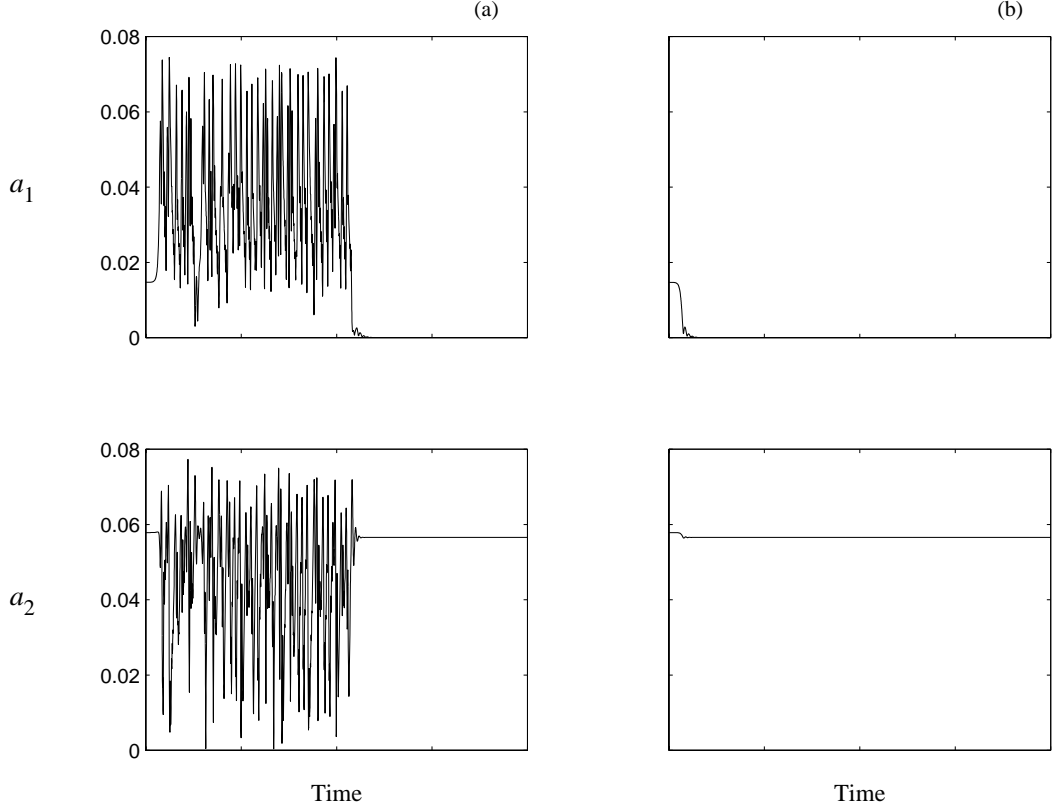
*Figure 5.* Time responses when $\delta = 1$, $\mu_1 = 0.0005$, $\mu_2 = 0.001$, $\nu_1 = 0.01$, $f = 0.0001$, and $\sigma_2 = 0.001740453$. Initial conditions on the unstable manifold of branch $AB$.

To investigate the nature of the dynamic solutions, we numerically integrated Equations (32–35) between $A$ and $G$ and found that the response is chaotic. Therefore, we analyzed the system between and in the neighborhood of points $A$ and $G$. In Figure 4, we show two-dimensional projections of the phase portraits and Poincaré sections for two values of $\sigma_2$ that lie in the region between points $A$ and $G$. Clearly, the system exhibits high-amplitude chaotic responses.

Next, we studied the system dynamics near point $A$. When $\sigma_2$ is increased beyond $A$, the response jumps to a chaotic attractor. However, when $\sigma_2$ is decreased, the chaotic response is maintained for a small region to the left of point $A$. Further decreases in $\sigma_2$ lead to the single-mode solution. Here, the chaotic attractor may be destroyed through a Shilnikov scenario or a boundary crisis [10]. In the presence of orbits homoclinic to a saddle-focus, Shilnikov's theorem predicts chaotic behavior on the outer side of the orbit if the ratio

$$r = \frac{|\rho|}{\lambda_1}$$

is less than one, where $\rho$ is the value of the real part of the stable complex conjugate eigenvalues and $\lambda_1$ is the value of the unstable real eigenvalue. We looked for orbits homoclinic to the saddle-focus close to point A. To this end, we searched for limit cycles by choosing initial conditions in both directions on the unstable manifolds of the saddle-focus on branch $AB$. In Figure 5, we show time traces of the responses. All initial conditions lead to the single-mode

9

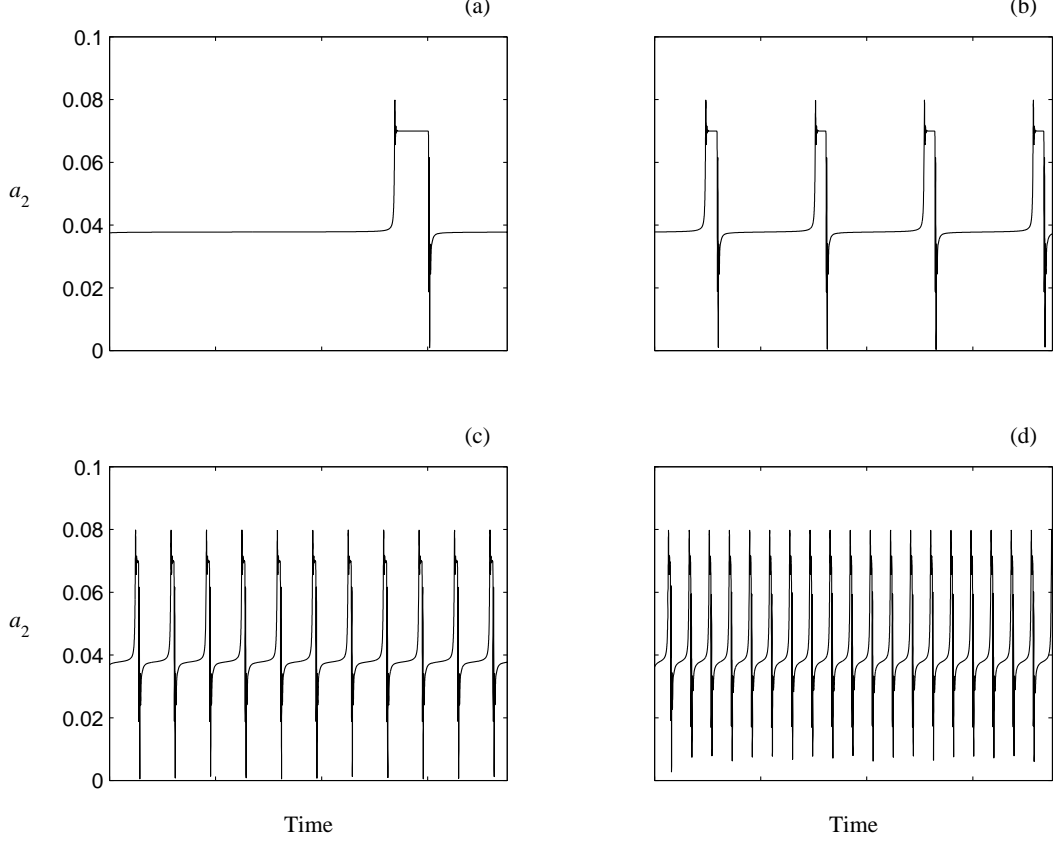| $\sigma_2$ | 0.001872 | 0.001899 | 0.001918 | 0.001930 | 0.001935 |
|---|---|---|---|---|---|
| $r$ | 1.10 | 1.59 | 2.74 | 7.42 | 242 |



*Figure 6.* Time evolution of the plant amplitude when $\delta = 1$, $\mu_1 = 0.0005$, $\mu_2 = 0.001$, $\nu_1 = 0.01$, and $f = 0.0001$. (a) $\sigma_2 = 0.003878056$, (b) $\sigma_2 = 0.00387801$, (c) $\sigma_2 = 0.0038775$, and (d) $\sigma_2 = 0.003876$.

solution. In the event that a homoclinic orbit existed, we monitored the ratio $r$. In Table 2, we list the value of the ratio $r$ as $A$ is approached. Since the value is greater than one and increasing, we concluded that a Shilnikov scenario is not possible. Therefore, the chaotic attractor is destroyed by a boundary crisis.

Finally, we investigated the system dynamics near point $G$, where the single-mode response undergoes a saddle-node bifurcation at $\sigma_2 = 0.003878544$. Beyond $G$, the system exhibits an intermittent response. The response of the plant alternates between two single-mode states: the old (ghost) solution near $G$ and the unstable solution on branch $AH$. As $\sigma_2$ is decreased, the frequency of intermittency increases, as illustrated in Figure 6. Chaos is reached through a type I intermittency.

Based on the frequency-response analysis, it appears that it is possible to implement the proposed absorber when $\delta < 0$ and the forcing amplitude is small. Consequently, we study
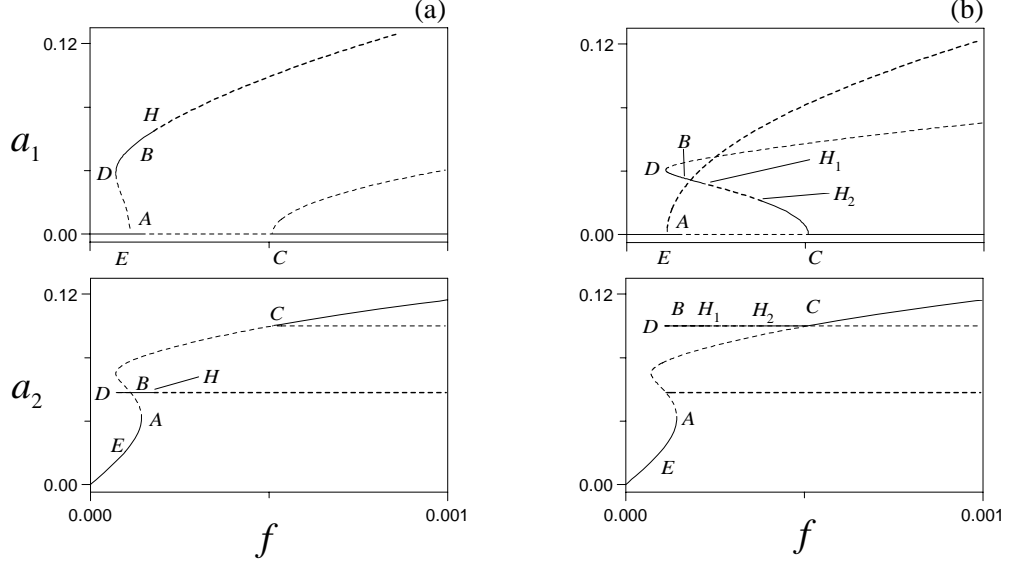
*Figure 7.* Force-response curves when $\mu_1 = 0.0005$, $\mu_2 = 0.001$, and $\nu_1 = 0.01$. (a) $\delta = -1$ and $\sigma_2 = -0.005$ and (b) $\delta = 1$ and $\sigma_2 = 0.005$. Solid (dotted) lines denote stable nodes (saddles) and bold-dashed lines denote unstable foci.

the effect of varying the forcing amplitude on the response of the system. In Figure 7, we display the force-response curves when $\mu_1 = 0.0005$, $\mu_2 = 0.001$, and $\nu_1 = 0.01$. The system exhibits a two-valued saturation phenomenon.

First, we analyze the case when $\delta = -1$ and $\sigma_2 = -0.005$, which is shown in Figure 7a. Initially, as $f$ is increased from zero and in the absence of large disturbances, the response consists of the single-mode solution, which is stable. The solution goes through a saddle-node bifurcation at $A$, leading to a stable two-mode solution at $B$. As $f$ is increased beyond $f_B$, the response of the directly excited mode saturates at the value $a_2^{(1)}$, and the response of the unexcited mode increases. At point $H$, the response experiences a subcritical Hopf bifurcation leading to a jump to a dynamic solution. When $f > f_C$, the system may be attracted to either the constant single-mode solution or to a two-mode dynamic solution. When $f$ is decreased, there are two possible paths for the solutions. If the initial conditions are small, the system response will consist of the single-mode solution. This solution loses stability through a subcritical pitchfork bifurcation at $f = f_C$. When $f < f_C$, the responses of both modes undergo jumps and are attracted to a dynamic solution. If the initial conditions are large, the system may be attracted directly to a dynamic solution. Because the Hopf bifurcation at $H$ is subcritical, a dynamic solution may coexist with the stable two-mode solution when $f < f_H$. If the constant two-mode solution is reached, then as $f$ is decreased, the solution will trace the curve $BD$ and will undergo a saddle-node bifurcation at $D$, leading to a jump to the single-mode solution at $E$.

In Figure 7b, we show force-response curves when $\delta = 1$ and $\sigma_2 = 0.005$. We note the emergence of a new region of dynamic solutions between the points $H_1$ and $H_2$. Furthermore, the subcritical pitchfork bifurcation at $C$ is replaced with a supercritical pitchfork bifurcation. When $0 < f < f_A$ and in the absence of large disturbances, the response consists of the
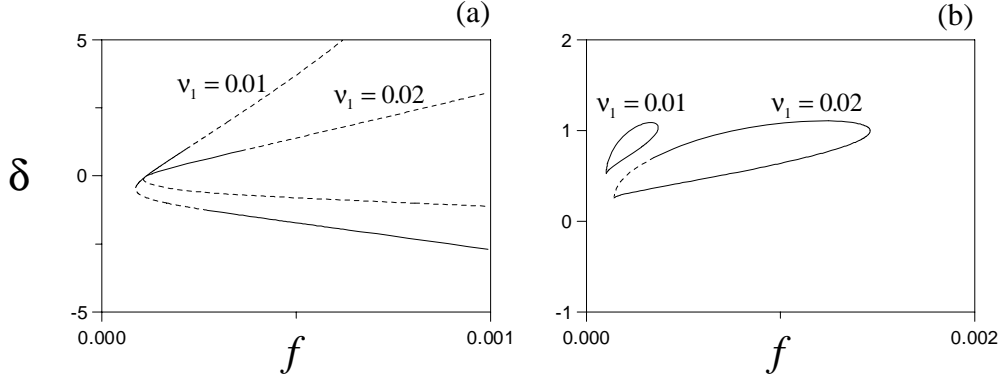
11

*Figure 8.* Projection of the Hopf bifurcation loci on the $\delta-f$ plane when $\mu_1 = 0.0005$ and $\mu_2 = 0.001$. (a) $\sigma_2 = -0.005$ and (b) $\sigma_2 = 0.005$. Solid (dotted) lines denote supercritical (subcritical) bifurcations.

single-mode solution. When $f > f_A$ and depending on the initial condition, the response may be attracted to either a dynamic or a constant solution in the region $BH_1$. In this case, the plant's amplitude may saturate at the value $a_2^{(2)}$. Subsequently, the solution undergoes a supercritical Hopf bifurcation at $H_1$. At $H_2$, the system experiences a reverse supercritical Hopf bifurcation after which the two-mode solution is attained. Then, the single-mode solution is reached through a supercritical pitchfork bifurcation at $C$. Similar results are expected when $f$ is decreased. However, a stable two-mode constant solution may be attained along branch $H_1D$.

Based on the results of the force-response analysis, we conclude that implementation of the absorber is possible only for small forcing amplitudes when $\delta < 0$. In Figure 8, we display the loci of the Hopf bifurcation points in the $\delta-f$ plane for different values of the detuning parameter $\nu_1$. It is clear that Hopf bifurcations that may lead to high-amplitude periodic or chaotic motions are possible.

## 4. Summary

We study the dynamics of a nonlinear vibration absorber. The absorber is based on a cubic feedback control law. We develop the equations of motion and obtain an approximate solution to the nonlinear differential equations using the method of multiple scales. Then, we conduct bifurcation analyses and investigate the performance of the control strategy. We show that a saturation phenomenon exists, and that it can be used, in a very limited range, for successful application of the technique. Additionally, we demonstrate the existence of dynamic solutions that may lead to high-amplitude or chaotic responses.

## Acknowledgments

## References

1. Sethna, P. R., 'Vibrations of dynamical systems with quadratic nonlinearities', *Journal of Applied Mechanics* **32**, 1965, 576–582.
2. Nayfeh, A. H., Mook, D. T., and Marshall, L. R., 'Nonlinear coupling of pitch and roll modes in ship motion', *Journal of Hydronautics* **7**, 1973, 145–152.
3. Haddow, A. G., Barr, A. D. S., and Mook, D. T., 'Theoretical and experimental study of modal interaction in a two degree-of-freedom structure', *Journal of Sound and Vibration* **97**, 1984, 451–473.
4. Balachandran, B. and Nayfeh, A. H., 'Observations of modal interactions in resonantly forced beam-mass structures', *Nonlinear Dynamics* **2**, 1991, 77–117.
5. Bajaj, A. K., Chang, S. I., and Johnson, J. M., 'Amplitude modulated dynamics of a resonantly excited autoparametric two degree-of-freedom system', *Nonlinear Dynamics* **5**, 1994, 433–457.
6. Banerjee, B., Bajaj, A. K., and Davies, P., 'Resonant dynamics of an autoparametric system: A study using higher order averaging', *International Journal of Non-Linear Mechanics* **31**, 1993, 21–39.
7. Oueini, S. S., Nayfeh, A. H., and Pratt, J. R., 'A nonlinear vibration absorber for flexible structures', *Nonlinear Dynamics* **15**, 1998, 259–282.
8. Pratt, J. R., Oueini, S. S., and Nayfeh, A. H., 'A Terfenol-D nonlinear vibration absorber', *Journal of Intelligent Material Systems and Structures*, 1999, to appear.
9. Nayfeh, A. H., *Perturbation Methods*, Wiley, New York, 1973.
10. Nayfeh, A. H. and Balachandran, B., *Applied Nonlinear Dynamics*, Wiley, New York, 1995.
11. Seydel, R., *Practical Bifurcation and Stability Analysis: From Equilibrium to Chaos*, Springer-Verlag, New York, 1994.